Sparse Imagination for Efficient Visual World Model Planning

Junha Chun¹*, Youngjoon Jeong²*, Taesup Kim^{2†}

¹Department of Electrical and Computer Engineering, Seoul National University ²Graduate School of Data Science, Seoul National University

Abstract

World model based planning has significantly improved decision-making in complex environments by enabling agents to simulate future states and make informed choices. However, ensuring the prediction accuracy of world models often demands substantial computational resources, posing a major challenge for real-time applications. This computational burden is particularly restrictive in robotics, where resources are severely constrained. To address this limitation, we propose a *Sparse* Imagination for Efficient Visual World Model Planning, which enhances computational efficiency by reducing the number of tokens processed during forward prediction. Our method leverages a sparsely trained vision-based world model based on transformers with randomized grouped attention strategy, allowing the model to adaptively adjust the number of tokens processed based on the computational resource. By enabling sparse imagination (rollout), our approach significantly accelerates planning while maintaining high control fidelity. Experimental results demonstrate that sparse imagination preserves task performance while dramatically improving inference efficiency, paving the way for the deployment of world models in real-time decision-making scenarios.

1 Introduction

By "imagining" future trajectories in a learned world model of the environment, agents can perform sophisticated decision making without trial-and-error in the real world [1, 2]. Recent world model advancements for visual control tasks, which necessitate reasoning over high-dimensional image observations, increasingly leverage high-level visual features derived from self-supervised vision models [3, 4, 5, 6]. For example, Zhou et al. [7] introduces a world model that predicts future Vision Transformer (ViT) patch tokens (DINO features) instead of pixels or single vector representation, enabling zero-shot planning for diverse tasks. By retaining spatially rich visual tokens, such approaches achieve strong generalization on control tasks with complex observations. A downside, however, is that using dozens or hundreds of visual tokens per image incurs high, quadratic computational cost during inference, especially if many rollout simulations are needed for planning each action. This raises a crucial question:

Can we retain the advantages of detailed visual world models while enhancing computational efficiency for planning?

In this paper, we address the above question by introducing the concept of *sparse imagination*, accelerating world model inference by deliberately using only a sparse subset of visual tokens during

^{*}These authors contributed equally.

[†]Corresponding author.

forward prediction. Our key insight is that ViT-based image representations contain redundancies [8, 9, 10, 11]—not all patch tokens are necessary for forward prediction or decision making.

To achieve this, we propose a random dropout-based token selection mechanism for the world model during inference that dynamically encodes and predicts only a subset of patch tokens. Furthermore, we train the world model using randomized grouped attention to accommodate dynamic token selection. The resulting system performs planning on the subset of latent patch tokens, reducing computational cost while maintaining competitive performance. The primary contributions of this work are as follows:

- We introduce a simple yet effective training and inference method for world models that leverages patch feature dropout to enable sparse visual imagination.
- Our sparse imagination approach, which utilizes randomly sampling token subsets, achieves substantial inference speedup while preserving competitive task performance across diverse visual control tasks compared to full-patch and single-vector baselines.
- Our work offers a thorough experimental analysis explaining the operational principles behind the success of the sparse imagination with planning framework.
- We show through a comparative study that simple random dropout performs comparably to or better than sophisticated token selection and merging methods.

2 Related Work

World Models for Control. World model based decision making, enabling agents to simulate futures for informed choices, has been a long-standing goal in reinforcement learning and robotics [12, 13]. The field transitioned from computationally heavy pixel-level models [14, 15] to latent dynamics models like PlaNet [1] and Dreamer [2, 16, 17], which achieved impressive results by leveraging planning and latent imagination. However, most existing latent world models compress entire images into relatively low-dimensional vectors. While compact, these representations can struggle to capture the fine-grained spatial information necessary for high-precision tasks, as evidenced by their performance on manipulation benchmarks [7, 18].

Visual Representations for Decision Making. A recent trend in decision making leverages powerful pre-trained visual encoders for rich state representations [5, 6]. While effective for representation learning, methods using a single image embedding (e.g., CLS token) from encoders like ResNet or ViT often lose crucial fine-grained spatial details, hindering performance on tasks requiring precise spatial understanding, such as manipulation [18, 7]. To address this, approaches using spatial features like ViT patch embeddings for decision making have been developed, exemplified by DINO-WM [7] which uses a set of DINO patch tokens as the state. Building on this paradigm, our work utilizes pre-trained ViT patch features for their spatial granularity. Our key innovation is an inference-time mechanism to drop these tokens during imagination, significantly enhancing computational efficiency. This motivates our central question: how can we retain the effectiveness of rich patch-based representations while substantially reducing computational cost on decision masking?

Vision Transformers and Token Efficiency. The quadratic scaling of ViT self-attention poses a significant computational challenge, particularly for sequential models like world models [19]. Improving inference efficiency via token reduction is thus a key vision research area. Existing methods employ diverse strategies such as learned/attention-based selection [20, 21, 22, 23, 24, 25], merging [26, 27, 28], and training-time dropout [29]. These demonstrate efficiency gains from ViT representation redundancy [8, 9, 10, 11]. In contrast, we present a patch-dropping method specifically for inference-time world model planning. Our approach uniquely applies dropout only during the imagination phase, enabling seamless integration with any transformer world model.

3 Methodology

We begin by describing the architecture and training procedure of our world model (Section 3.1), followed by introducing *sparse imagination*, which incorporates patch token dropout for efficient model predictive control (MPC) rollouts (Section 3.2).

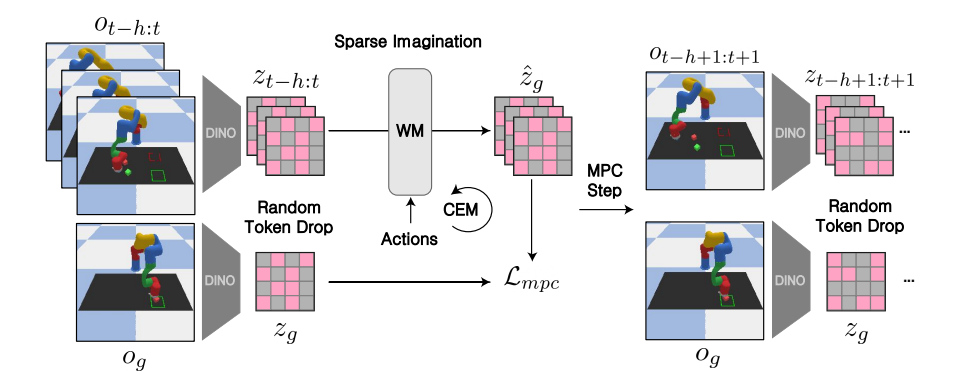


Figure 1: **Sparse Imagination.** We propose an accelerated strategy for visual world model based planning with sparse imagination, leveraging a patch token dropout mechanism to achieve efficient model predictive control (MPC) rollouts during inference. At each iteration of MPC, a random subset of visual patches is selected, and predictions are generated exclusively based on these sampled patches. Actions are optimized using the Cross-Entropy Method (CEM) by evaluating their predicted outcomes against the goal in latent space, calculated solely from the selected patches. This random dropout pattern is dynamically updated at every MPC iteration, thereby enhancing the model's robustness.

3.1 World Model

Our world model is composed of two key modules: (1) a pre-trained image encoder g_{ϕ} (e.g., DINO) generating visual latent patch tokens from observations, and (2) a transformer-based world model f_{θ} predicting future latent tokens based on historical observations and actions. The image encoder remains fixed during training to ensure stable visual representations, while the transformer-based world model learns temporal dynamics. Structured as a causal transformer decoder, the world model allows each token to attend only to tokens from prior time steps, enabling efficient sequence modeling.

Specifically, given an image observation $o_t \in \mathbb{R}^{H \times W \times 3}$ at time t, the image encoder g_ϕ extracts visual features $z_t \in \mathbb{R}^{H_p \times W_p \times D}$, where the number of visual tokens is $N = H_p \times W_p$. The world model f_θ predicts future features z_{t+1} using a temporal context of visual tokens and actions: $z_{t+1} = f_\theta(z_{t-h:t}, a_{t-h:t})$, with a history length of h+1. Our model predicts dynamics within the pre-trained DINO feature space. Actions and proprioceptive information, when available, are linearly projected and concatenated to visual tokens along the feature dimension. The world model training is guided by minimizing the mean squared error (MSE) prediction loss:

$$\mathcal{L}_{wm} = \frac{1}{N} \sum_{i=1}^{N} ||\hat{z}_{t+1,i} - z_{t+1,i}||^2,$$
 (1)

where i and N represent token index and the total visual tokens per frame, respectively. An optional decoder, detached from gradient updates, can be trained separately for visualization purposes.

To enhance generalization and robustness when only sparse subsets of tokens are provided as inputs, we introduce a randomized grouping strategy during training as depicted in Fig. 2. Specifically, visual tokens from each frame are randomly partitioned into two groups. This approach ensures different subset patterns during training, promoting adaptability across different levels of sparsity. To implement this, we apply attention masks within the transformer layers, restricting token interactions exclusively to those within the same spatial group while maintaining temporal consistency. By enforcing this structured token separation, our model learns to process arbitrary subsets of visual tokens while optimizing for the same prediction loss, ultimately improving its ability to generalize across varying input conditions.

3.2 Sparse Imagination for MPC

For planning with the world model, we utilize MPC using the Cross-Entropy Method (CEM) for trajectory optimization. At each MPC step, candidate action sequences $\{a_{t:t+H-1}\}$ are sampled

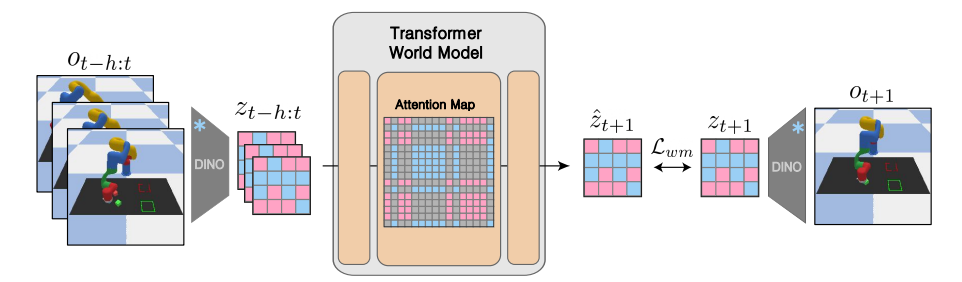


Figure 2: Randomized Grouped Attention Strategy. We introduce a randomized grouping strategy during training in order to generalize to arbitrary subsets of input tokens. Visual tokens from each frame are randomly partitioned into two spatial groups, with the number of tokens in the first group uniformly sampled. Attention masks within transformer layers constrain interactions to occur only among tokens within the same spatial group, and this grouping remains consistent across time steps. Consequently, the model becomes capable of processing varying subsets of visual tokens effectively, while optimizing the same prediction objective. We demonstrate its necessity in the ablation studies.

from a distribution. The trained world model f_{θ} then predicts future states by iteratively rolling out these action sequences from the current state. In a goal-conditioned setting, candidate sequences are evaluated through an objective such as the MSE loss between the predicted state features and a specified goal state:

$$\mathcal{L}_{\text{mpc}} = ||\hat{z}_{t+H} - z_q||^2. \tag{2}$$

The distribution of candidate actions is subsequently updated based on the top-performing sequences. This iterative optimization continues for a predefined iteration step M, after which the optimized action sequence is executed in the environment.

However, MPC can be computationally intensive due to significant amount of world model predictions. Specifically, world model rollout occurs $K \times M \times H$ times every MPC step, where the number of candidate sequences is K and planning horizon is K. Moreover, this computational cost scales exponentially with the number of visual tokens, making real-time execution increasingly challenging. Since attention layers in the world model are the primary source of this computational burden, reducing the number of tokens processed is crucial for improving MPC efficiency.

We address this problem through *sparse imagination*. Given that our model is explicitly trained to operate on arbitrary token subsets, we implement random token dropout during MPC planning as shown in Fig. 1. At each MPC step, we randomly generate a token dropout mask characterized by a dropout fraction $p \in [0,1)$ of the user's choice, denoting the proportion of tokens to discard, keeping randomly sampled (1-p)N tokens. Sparse rollout imagination can effectively reduce redundant computations and improve planning efficiency. Planning a single step might fall to wrong direction when dropping key features but has minimal impact on task performance since it can recover from failures by re-sampling at each planning iteration. The dropout fraction p serves as a controllable parameter balancing computational speed and task accuracy. We empirically evaluate and analyze this trade-off in Section 4.

4 Experiments and Analysis

4.1 Implementation Details

Environments and Datasets. We conduct our evaluations on six datasets (See Fig. 3), each designed to test different aspects of visual planning: maze-based navigation (Pointmaze, Wall), tabletop object pushing (PushT), manipulation of deformable objects using robotic arms (Rope, Granular), and precise robotic manipulation tasks (Block Pushing). In each environment, the goal is reaching a target observation randomly sampled as a desired goal state, starting from initial positions. All observations consist of RGB images with a resolution of 224×224 .

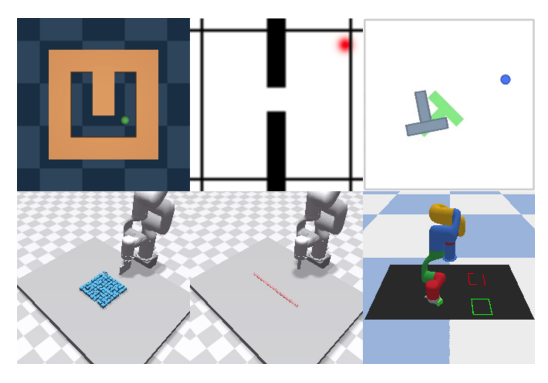
Baselines. We evaluate our approach across several visual control domains and compare it against key baselines. The primary baselines include: (1) a **Full-Patch** world model, which shares the

Table 1: Performance results (Mean Success Rate, %) across different environments with varying drop ratios.

| | Pointmaze (60 evals) | Wall (60 evals) | PushT (60 evals) | Granular (20 evals) | Rope (30 evals) | Block Pushing (50 evals) | |
|--------------|----------------------|--------------------|---------------------|------------------------|--------------------|-----------------------------|--|
| Full | 98.3 | 85.0 | 75.0 | 75.0 | 63.3 | 22.0 | |
| CLS | 96.7 | 91.7 | 43.3 | 20.0 | 36.7 | 16.0 | |
| Drop (Ratio) | | | | | | | |
| 10% | 91.7 | 93.3 | 78.3 | 80.0 | 73.3 | 28.0 | |
| 20% | 90.0 | 95.0 | 70.0 | 80.0 | 66.7 | 16.0 | |
| 30% | 98.3 | 93.3 | 61.7 | 85.0 | 70.0 | 18.0 | |
| 40% | 96.7 | 93.3 | 56.7 | 70.0 | 76.7 | 18.0 | |
| 50% | 100.0 | 95.0 | 70.0 | 60.0 | 73.3 | 20.0 | |
| 60% | 83.3 | 91.7 | 46.7 | 70.0 | 70.0 | 20.0 | |
| 70% | 70.0 | 93.3 | 28.3 | 55.0 | 53.3 | 20.0 | |
| 80% | 73.3 | 90.0 | 21.7 | 50.0 | 66.7 | 24.0 | |
| 90% | 71.7 | 86.7 | 20.0 | 40.0 | 50.0 | 12.0 | |

Table 2: Planning time and change compared to Full baseline for different environments at various drop ratios.

| | Pointmaze | | Wall | | PushT | | Block Pushing | | |
|--------------|---------------------------|--------------|---------------------------|--------------|---------------------------|--------------|---------------------------|--------------|--|
| | Planning Time (s/iter) | Change (%) | |
| Full CLS | 184 49 | 0.0 -73.4 | 79 40 | 0.0 -49.4 | 173 32 | 0.0 -81.5 | 297 163 | 0.0 -45.1 | |
| Drop (Ratio) | | | | | | | | | |
| 10% | 165 | -10.3 | 73 | -7.6 | 149 | -13.9 | 278 | -6.4 | |
| 20% | 141 | -23.4 | 69 | -12.7 | 131 | -24.3 | 259 | -12.8 | |
| 30% | 126 | -31.5 | 65 | -17.7 | 114 | -34.1 | 240 | -19.2 | |
| 40% | 106 | -42.4 | 62 | -21.5 | 97 | -43.9 | 214 | -27.9 | |
| 50% | 93 | -49.5 | 53 | -32.9 | 82 | -52.6 | 208 | -30.0 | |
| 60% | 80 | -56.5 | 50 | -36.7 | 69 | -60.1 | 200 | -32.7 | |
| 70% | 69 | -62.5 | 46 | -41.8 | 59 | -65.9 | 184 | -38.0 | |
| 80% | 56 | -69.6 | 46 | -41.8 | 49 | -71.7 | 175 | -41.1 | |
| 90% | 48 | -73.9 | 42 | -46.8 | 38 | -78.0 | 167 | -43.8 | |



model across six distinct environments, arranged as follows (left-to-right, top-to-bottom): Pointmaze, Wall, PushT, Granular, Rope, and Block Pushing.

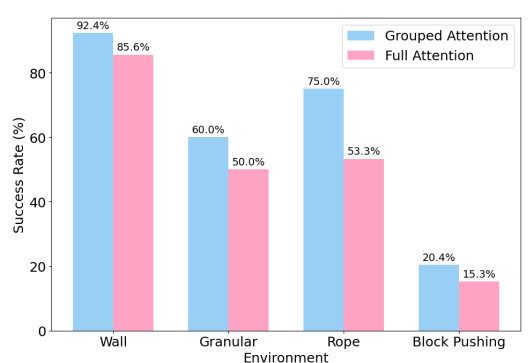


Figure 3: Environments. We assess the world Figure 4: Contribution of grouped attention during pretraining to planning. We compare the average planning success rates achieved by grouped attention and full attention under various drop ratios, highlighting the benefit of grouped attention.

same architecture as ours but utilizes all patches during planning (i.e., p = 0) and applies positional encoding to each patch—representing a high-fidelity yet computationally expensive setting; and (2) a CLS-Token world model, which employs only the global CLS token from the DINO encoder as the

visual representation, thereby offering a single-vector representation baseline. These two baselines are based on the approach presented in [7]. Our analysis focuses on the trade-offs between these approaches in terms of task performance and inference efficiency.

Planning Setup. We apply MPC-CEM to the PointMaze, Wall, PushT, and Block Pushing environments, whereas the Granular and Rope environments employ the CEM approach due to the prolonged processing time in the deformable environment. Here, CEM refers to optimizing a fixed sequence of actions without intermediate corrections or replanning during execution, whereas MPC-CEM denotes optimization using CEM with replanning at each step in a receding horizon manner. In all environments, the MPC horizon is set to H=5. For each optimization step, we sample 100 candidate actions and select the top 10 based on the distance computed between the current and goal observations. Note that in sparse imagination scenarios, the distance is computed using only a subset of patches rather than the full patches. Each CEM optimization is performed for 10 steps. For the Wall and Block Pushing environments, the maximum number of MPC iterations is set to 10, while for Pointmaze and PushT, we set the maximum iterations to 15.

4.2 Performance and Computational Efficiency

The experimental outcomes are summarized across two primary tables. Table 1 reports the Success Rate (SR) to the goal across various environments with various token dropout ratios. We evaluated 60 episodes for PointMaze, Wall, and PushT, and 50 episodes for Block Pushing. Due to the prolonged interaction time in the Deformable Environment, Rope and Granular are evaluated on 30 and 20 episodes, respectively. Table 2 outlines the associated planning times, highlighting percentage reductions compared to the **Full-Patch** model. Employing moderate dropout ratios (typically between 10% and 50%) yields comparable or improved performance relative to the **Full-Patch** baseline, with substantial reductions in planning times. For example, around a dropout level 50%, planning time reductions approach 30–50% in tested environments. Although dropout models remain slower than the **CLS-Token** baseline, their predictive performance significantly surpasses the CLS-based method.

Task Difficulty and Scene Complexity. This tendency is more pronounced in complex or difficult environments (Granular, Rope, PushT, Block Pushing). In spatially demanding scenes (Granular, Rope), the CLS-Token baseline (20.0%, 36.7% success) fails to capture necessary details. In contrast, our patch dropout approach with moderate ratios achieves significantly higher success (up to 85.0%, 76.7%), demonstrating that a pruned token set better preserves critical spatial information than a single global token. For high-difficulty tasks (PushT, Block Pushing), dropout also substantially outperforms CLS (43.3%, 16.0%) and performs comparably to or slightly better than the Full-Token baseline (e.g., 75.0% for Full in PushT), validating the efficacy of planning with token subsets.

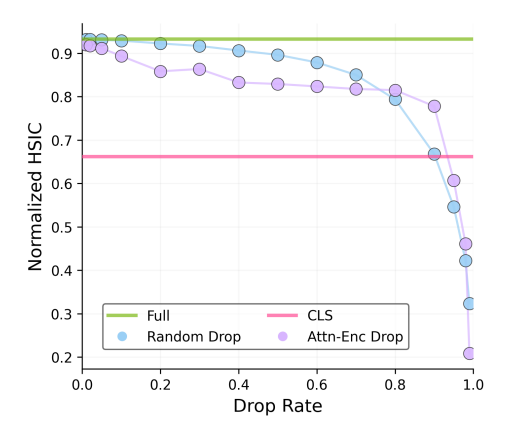
Dropout Ratios. Generally, performance remains stable compared to using full patches for planning, with dropout ratios up to approximately 50%, after which it deteriorates, although the degree of degradation varies by dataset. This suggests that excessively high dropout rates result in the loss of patches containing critical information required for effective task completion.

Planning Time Improvements. In addition to improved performance, our patch dropout method offers significant computational benefits. For instance, in the PushT environment, planning time per iteration drops from 173 seconds (**Full-Patch** baseline) to 82 seconds at a 50% dropout ratio—52.6% reduction. Similar improvements in planning time are observed across other environments such as Wall, PushT, and Block Pushing. Although the **CLS-Token** baseline provides even faster inference times, its dramatic drop in performance—especially in complex and high-difficulty scenarios—renders it less viable for practical applications.

4.3 Empirical Insights into Sparse Imagination

We validate our approach by showing experimentally that a subset of visual patch tokens is sufficient for effective planning, making the full patch tokens unnecessary.

Information-Theoretic Analysis. We measured the mutual information between visual tokens and ground-truth states using normalized Hilbert-Schmidt Independence Criterion (nHSIC) [30] to assess token dropout's impact on information quality. Experiments across various dropout rates (Fig. 5)



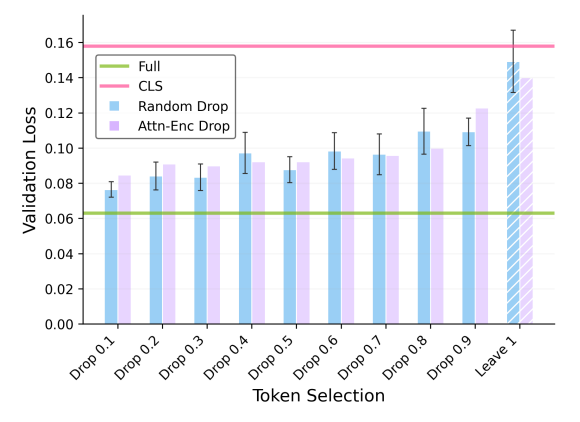


Figure 5: **nHSIC** between visual tokens and **environment states.** nHSIC scores with respect to dropout rate for random dropout compared to Full, CLS, and Attention-Encoder dropout in Granular dataset.

Figure 6: **Attentive probing performance.** Validation losses for state prediction with attentive probing compared to Attention-Encoder baseline in Granular dataset.

show that high HSIC scores are maintained even under substantial dropout, indicating minimal loss of critical state information. Furthermore, even retaining just 10% of tokens yields higher nHSIC than the CLS token, which is intended to capture global image information.

Attentive Probing Analysis. To further validate our findings, we trained an attentive probing module [31] to assess how well tokens predict ground-truth states (details in Fig. 6 and Appendix). While probing errors modestly increase with higher dropout rates, this suggests random subsets still encode sufficient information. Furthermore, a single random token shows predictive accuracy comparable (albeit with variance) to the CLS token, indicating state information is distributed across tokens.

Role of Randomized Grouped Attention. While a subset of patch tokens contains sufficient state information for accelerated planning via token dropout, predicting solely on this subset can introduce errors. We show that training the world model with randomized grouped attention can reduce these errors. Our comparison of full attention and grouped attention models shows that grouped attention lowers the mean relative L2 distance of subset predictions (0.016) compared to full attention (0.036). This reduction in prediction error aligns with the improved planning performance observed with grouped attention under token dropout (Fig. 4). Experimental details on attention mechanisms are provided in the Appendix.

Planning Robustness. Although randomized grouped attention reduces prediction errors on the token subset under dropout, complete elimination is not achieved. Consistent with prior studies showing CEM's robustness to noise and uncertainties [32, 33, 34], we claim this remaining error sufficient for effective planning, based on the experimental results (Table 1). Detailed experiments evaluating CEM's performance with visual token errors in our framework are in the Appendix.

4.4 Token Dropout Methods

We investigated whether more sophisticated token dropout strategies can improve planning performance. To this end, we empirically evaluated the average planning success rate of various token selection and merging methods across different drop ratios. We compare uniform baselines against more advanced learned or structured approaches. As uniform baselines within the MPC framework, we consider **Random** (our standard setting), which resamples the dropout mask at each MPC step, and **Fixed**, which uses a single mask throughout. Both sample tokens uniformly. Beyond these, we evaluate:

• LHS [35]: Employs Latin Hypercube Sampling for spatially uniform sampling at each step.

- LTRP [21]: Trains a score network to predict patch importance using the reconstruction loss from pre-trained MAE [36].
- Attention-Encoder: Derives token importance from the attention map between the CLS and patch tokens of a DINO encoder, where higher attention weights indicate greater importance. This is a common practice in pruning-based prior research [23, 24, 25]. We use attention map of the final layer of pretrained DINO.
- STAR [25]: Calculates importance scores by fusing intra-layer scores from CLS attention and inter-layer scores from modified Layer-wise Relevance Propagation (LRP; [37]). We select important tokens based on the final layer score of DINO encoder.
- Attention-WM: Evaluates importance based on the average attention weight a token receives as a query from others in each layer. Importance is determined by averaging the attention maps across all layers.
- Agglomerative Token Clustering (ATC) [28]: Utilizes agglomerative clustering to group tokens, followed by average pooling. For planning, we first apply agglomerative clustering to the context observation image features to predict future clustered features. In parallel, agglomerative clustering is performed on the goal image features. The distance between the predicted future and the goal is then determined via Hungarian matching between the predicted future clusters and the goal clusters, and this distance guides the planning process.

Table 3: The average planning success rate (%) achieved by various token dropout and merging methods under different drop ratios. Our results suggest that no method achieves significantly superior performance compared to the Random sampling.

| Туре | Methods | Pointmaze | Wall | PushT | Granular | Rope | Block Pushing |
|-------------------------|-------------------|-----------|------|-------|----------|------|---------------|
| | Random | 85.8 | 93.8 | 50.4 | 70.0 | 73.3 | 20.5 |
| Random Sampling | Fixed | 87.1 | 85.0 | 47.4 | - | - | 16.5 |
| | LHS [35] | 84.2 | 92.5 | 49.6 | - | - | 21.0 |
| Learning-Based Pruning | LTRP [21] | 79.2 | 94.6 | 40.9 | 65.0 | 42.2 | 16.5 |
| | Attention-Encoder | 79.2 | 97.1 | 43.9 | 68.4 | 63.3 | 20.5 |
| Attention-Based Pruning | STAR [25] | 82.9 | 85.8 | 46.9 | - | 63.3 | 17.0 |
| | Attention-WM | 80.0 | 93.8 | 44.3 | - | 61.7 | 16.5 |
| Cluster & Merging | ATC [28] | 78.3 | 81.2 | 39.1 | 25.0 | 18.3 | 11.5 |

Across diverse datasets, our empirical results consistently demonstrate that none of the evaluated token selection methods achieve performance significantly superior to the **Random** (Table 3). We visualize the actual dropout patterns of different token dropout methods in Figure 7 to illustrate their characteristics. Further experimental results are provided in the Appendix.

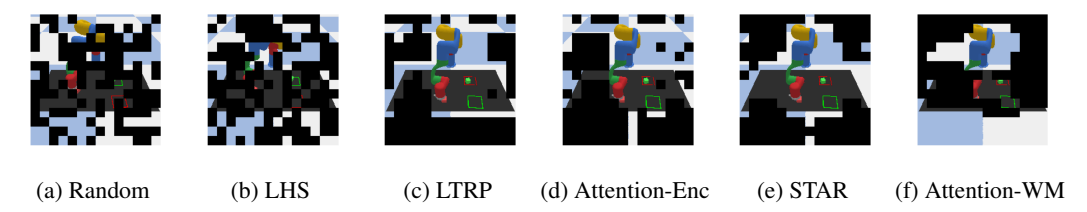


Figure 7: Visualization of token dropout patterns for different token reduction methods. Patterns at 50% dropout ratio are shown from left to right for Random, LHS, LTRP, Attention-Encoder, STAR, and Attention-WM.

Spatial Uniformity Does Not Matter. Comparing **LHS** (enforcing spatial uniformity) with **Random** reveals that a purely spatial selection criterion offers no significant advantage in planning success rates. Contrary to an intuition that uniform spatial coverage might be beneficial, our results suggest simply distributing selections evenly is insufficient for prioritizing tokens critical for effective planning.

Random vs. Sophisticated Dropout Methods. We observe that various token dropout methods do not yield significantly superior performance compared to random dropout. We attribute this to two factors: 1) the substantial inherent redundancy of ViT representations [8, 9, 10, 11], and 2) our world model's training design using randomized grouped attention, which encourages learning to predict from limited token subsets by leveraging this information redundancy.

Random vs. Fixed Dropout Patterns during Planning Steps. Investigating token reduction strategies, we compared Random and Fixed dropout patterns. Random dropout offers a key robustness advantage in sparse imagination: its stochastic nature enables resampling, facilitating recovery from temporarily dropping essential information in subsequent MPC iterations. This contrasts with fixed patterns, which lack this recovery mechanism. This robustness could explain Random's empirical outperformance relative to Fixed.

Dropout vs. Clustering-Based Merging. Lastly, we compare our stochastic dropout (Random) with clustering-based token merging (ATC), which also aims to compress scene representations. Table 3 shows ATC significantly underperforming Random, a gap widening with increased compression. This likely stems from clustering aggregating patches in a manner that diverges from the original distribution and loses fixed spatial positions, hindering world model generalization. Computationally, ATC is significantly slower than Random (up to 268.0% increase planning time), primarily due to the quadratic complexity of clustering and the need for additional spatial matching procedures. Random dropout, conversely, relies on efficient, constant-time index sampling that maintains spatial fidelity. Further details on the clustering implementation and full experimental results for ATC's planning time are provided in the Appendix.

Information and Probing Analysis of Token Dropout Methods. HSIC analysis indicates that attention-based selection baselines (e.g., Attention-Encoder) do not achieve significantly higher mutual information than random dropout (Fig. 5). Their often poor nHSIC correlation suggests a misalignment between tokens highlighted by the DINO encoder's attention and those critical for capturing the state. Also, in attention probing (Fig. 6), compared with the **Attention-Encoder** baseline, random dropout shows consistently similar performance, questioning the need of additional token selection methods for planning.

5 Conclusion

In this paper, we introduce a novel approach for computationally efficient planning using sparse imagination, implemented via patch token dropout in transformer-based world models. Our method significantly reduces computational complexity during planning by processing subsets of visual tokens, while incurring only minimal loss in predictive performance. This approach enables fast control in complex visual environments, effectively balancing computational efficiency and task accuracy. Empirical evaluations across various settings confirm the effectiveness and robustness of sparse imagination. Furthermore, our extensive experiments analyze and provide insights into why the framework of sparse imagination with planning is viable. Lastly, our comparative study experimentally demonstrates that diverse token selection strategies do not significantly outperform simple random sampling, suggesting the sufficiency of simple random sampling for planning within this framework.

Limitations Our work's key limitation is that experiments were conducted on simulated datasets rather than real-world data. Additionally, although random token dropout is shown effective in reducing computational overhead, the dropout rate requires adjustments based on the specific environment and computational requirements. Finally, our experiments were primarily conducted using a DINO encoder, thus exploring behaviors of other pretrained vision encoders with different representational properties applied to our work is an interesting direction for future research.

References

- [1] Danijar Hafner, Timothy Lillicrap, Ian Fischer, Ruben Villegas, David Ha, Honglak Lee, and James Davidson. Learning latent dynamics for planning from pixels. In Kamalika Chaudhuri and Ruslan Salakhutdinov, editors, *Proceedings of the 36th International Conference on Machine Learning*, volume 97 of *Proceedings of Machine Learning Research*, pages 2555–2565. PMLR, 09–15 Jun 2019.
- [2] Danijar Hafner, Timothy Lillicrap, Jimmy Ba, and Mohammad Norouzi. Dream to control: Learning behaviors by latent imagination. *arXiv* preprint arXiv:1912.01603, 2019.
- [3] Mathilde Caron, Hugo Touvron, Ishan Misra, Hervé Jégou, Julien Mairal, Piotr Bojanowski, and Armand Joulin. Emerging properties in self-supervised vision transformers. In *Proceedings of the IEEE/CVF international conference on computer vision*, pages 9650–9660, 2021.
- [4] Maxime Oquab, Timothée Darcet, Théo Moutakanni, Huy Vo, Marc Szafraniec, Vasil Khalidov, Pierre Fernandez, Daniel Haziza, Francisco Massa, Alaaeldin El-Nouby, et al. Dinov2: Learning robust visual features without supervision. *arXiv preprint arXiv:2304.07193*, 2023.
- [5] Suraj Nair, Aravind Rajeswaran, Vikash Kumar, Chelsea Finn, and Abhinav Gupta. R3m: A universal visual representation for robot manipulation. *arXiv preprint arXiv:2203.12601*, 2022.
- [6] Tete Xiao, Ilija Radosavovic, Trevor Darrell, and Jitendra Malik. Masked visual pre-training for motor control. arXiv preprint arXiv:2203.06173, 2022.
- [7] Gaoyue Zhou, Hengkai Pan, Yann LeCun, and Lerrel Pinto. DINO-WM: World models on pre-trained visual features enable zero-shot planning. *arXiv preprint arXiv:2411.04983*, 2024.
- [8] Maithra Raghu, Thomas Unterthiner, Simon Kornblith, Chiyuan Zhang, and Alexey Dosovitskiy. Do vision transformers see like convolutional neural networks? *Advances in neural information processing systems*, 34:12116–12128, 2021.
- [9] Bowen Pan, Rameswar Panda, Yifan Jiang, Zhangyang Wang, Rogerio Feris, and Aude Oliva. Ia-red2: Interpretability-aware redundancy reduction for vision transformers. *Advances in neural information processing systems*, 34:24898–24911, 2021.
- [10] Tianlong Chen, Zhenyu Zhang, Yu Cheng, Ahmed Awadallah, and Zhangyang Wang. The principle of diversity: Training stronger vision transformers calls for reducing all levels of redundancy. In *Proceedings of the IEEE/CVF Conference on Computer Vision and Pattern Recognition*, pages 12020–12030, 2022.
- [11] Manjin Kim, Paul Hongsuck Seo, Cordelia Schmid, and Minsu Cho. Learning correlation structures for vision transformers. In *Proceedings of the IEEE/CVF conference on computer vision and pattern recognition*, pages 18941–18951, 2024.
- [12] Leslie P. Kaelbling, Michael L. Littman, and Anthony R. Cassandra. Planning and acting in partially observable stochastic domains. *Artificial Intelligence*, 101(1-2):99–134, 1996.
- [13] David Ha and Jürgen Schmidhuber. World models. 2018.
- [14] Chelsea Finn, Ian Goodfellow, and Sergey Levine. Unsupervised learning for physical interaction through video prediction. *Advances in neural information processing systems*, 29, 2016.
- [15] Frederik Ebert, Chelsea Finn, Sudeep Dasari, Annie Xie, Alex Lee, and Sergey Levine. Visual foresight: Model-based deep reinforcement learning for vision-based robotic control. *arXiv* preprint arXiv:1812.00568, 2018.
- [16] Danijar Hafner, Timothy Lillicrap, Mohammad Norouzi, and Jimmy Ba. Mastering atari with discrete world models. arXiv preprint arXiv:2010.02193, 2020.
- [17] Danijar Hafner, Jurgis Pasukonis, Jimmy Ba, and Timothy Lillicrap. Mastering diverse domains through world models. *arXiv preprint arXiv:2301.04104*, 2023.

- [18] Nikolaos Tsagkas, Andreas Sochopoulos, Duolikun Danier, Sethu Vijayakumar, Chris Xiaoxuan Lu, and Oisin Mac Aodha. When pre-trained visual representations fall short: Limitations in visuo-motor robot learning, 2025.
- [19] Alexey Dosovitskiy, Lucas Beyer, Alexander Kolesnikov, Dirk Weissenborn, Xiaohua Zhai, Thomas Unterthiner, Mostafa Dehghani, Matthias Minderer, Georg Heigold, Sylvain Gelly, et al. An image is worth 16x16 words: Transformers for image recognition at scale. *arXiv* preprint *arXiv*:2010.11929, 2020.
- [20] Yongming Rao, Wenliang Zhao, Benlin Liu, Jiwen Lu, Jie Zhou, and Cho-Jui Hsieh. Dynamicvit: Efficient vision transformers with dynamic token sparsification. Advances in neural information processing systems, 34:13937–13949, 2021.
- [21] Yang Luo, Zhineng Chen, Peng Zhou, Zuxuan Wu, Xieping Gao, and Yu-Gang Jiang. Learning to rank patches for unbiased image redundancy reduction. In *Proceedings of the IEEE/CVF Conference on Computer Vision and Pattern Recognition*, pages 22831–22840, 2024.
- [22] Hongxu Yin, Arash Vahdat, Jose M Alvarez, Arun Mallya, Jan Kautz, and Pavlo Molchanov. A-vit: Adaptive tokens for efficient vision transformer. In *Proceedings of the IEEE/CVF conference on computer vision and pattern recognition*, pages 10809–10818, 2022.
- [23] Youwei Liang, G E Chongjian, Zhan Tong, Yibing Song, Jue Wang, and Pengtao Xie. EViT: Expediting vision transformers via token reorganizations. In *International Conference on Learning Representations*, October 2021.
- [24] Zhenyu Wang, Hao Luo, Pichao Wang, Feng Ding, Fan Wang, and Hao Li. Vtc-lfc: Vision transformer compression with low-frequency components. Advances in Neural Information Processing Systems, 35:13974–13988, 2022.
- [25] Yuyao Zhang, Lan Wei, and Nikolaos Freris. Synergistic patch pruning for vision transformer: Unifying intra- & inter-layer patch importance. In *The Twelfth International Conference on Learning Representations*, October 2024.
- [26] Daniel Bolya, Cheng-Yang Fu, Xiaoliang Dai, Peizhao Zhang, Christoph Feichtenhofer, and Judy Hoffman. Token merging: Your vit but faster. *arXiv preprint arXiv:2210.09461*, 2022.
- [27] Zhanzhou Feng and Shiliang Zhang. Efficient vision transformer via token merger. *IEEE Transactions on Image Processing*, 32:4156–4169, 2023.
- [28] Joakim Bruslund Haurum, Sergio Escalera, Graham W Taylor, and Thomas B Moeslund. Agglomerative token clustering. In *European Conference on Computer Vision*, pages 200–218. Springer, 2024.
- [29] Yue Liu, Christos Matsoukas, Fredrik Strand, Hossein Azizpour, and Kevin Smith. Patchdropout: Economizing vision transformers using patch dropout. In *Proceedings of the IEEE/CVF Winter Conference on Applications of Computer Vision*, pages 3953–3962, 2023.
- [30] A. Gretton, O. Bousquet, AJ. Smola, and B. Schölkopf. Measuring statistical dependence with hilbert-schmidt norms. Technical Report 140, Max Planck Institute for Biological Cybernetics, Tübingen, Germany, June 2005.
- [31] Adrien Bardes, Quentin Garrido, Jean Ponce, Michael Rabbat, Yann LeCun, Mahmoud Assran, and Nicolas Ballas. Revisiting feature prediction for learning visual representations from video. *arXiv:2404.08471*, 2024.
- [32] Pieter-Tjerk De Boer, Dirk P Kroese, Shie Mannor, and Reuven Y Rubinstein. A tutorial on the cross-entropy method. *Annals of operations research*, 134:19–67, 2005.
- [33] Jiaqiao Hu and Ping Hu. On the performance of the cross-entropy method. In *Proceedings of the 2009 winter simulation conference (WSC)*, pages 459–468. IEEE, 2009.
- [34] Sahin Lale, Peter I Renn, Kamyar Azizzadenesheli, Babak Hassibi, Morteza Gharib, and Anima Anandkumar. Falcon: Fourier adaptive learning and control for disturbance rejection under extreme turbulence. *npj Robotics*, 2(1):6, 2024.

- [35] Michael D McKay, Richard J Beckman, and William J Conover. A comparison of three methods for selecting values of input variables in the analysis of output from a computer code. *Technometrics*, 42(1):55–61, 2000.
- [36] Kaiming He, Xinlei Chen, Saining Xie, Yanghao Li, Piotr Dollár, and Ross Girshick. Masked autoencoders are scalable vision learners. In *Proceedings of the IEEE/CVF conference on computer vision and pattern recognition*, pages 16000–16009, 2022.
- [37] Hila Chefer, Shir Gur, and Lior Wolf. Transformer interpretability beyond attention visualization. In *Proceedings of the IEEE/CVF conference on computer vision and pattern recognition*, pages 782–791, 2021.
- [38] Justin Fu, Aviral Kumar, Ofir Nachum, George Tucker, and Sergey Levine. D4rl: Datasets for deep data-driven reinforcement learning, 2020.
- [39] Cheng Chi, Siyuan Feng, Yilun Du, Zhenjia Xu, Eric A. Cousineau, Benjamin Burchfiel, and Shuran Song. Diffusion policy: Visuomotor policy learning via action diffusion. *ArXiv*, abs/2303.04137, 2023.
- [40] Kaifeng Zhang, Baoyu Li, Kris Hauser, and Yunzhu Li. Adaptigraph: Material-adaptive graph-based neural dynamics for robotic manipulation. *ArXiv*, abs/2407.07889, 2024.
- [41] Fen Xia, Tie-Yan Liu, Jue Wang, Wensheng Zhang, and Hang Li. Listwise approach to learning to rank: theory and algorithm. In *Proceedings of the 25th international conference on Machine learning*, pages 1192–1199, 2008.

A Implementation Details

Dataset Size # Frames History len Frame skip Train epoch Pointmaze 2000 100 3 5 10 Wall 50 3 5 100 1920 3 **PushT** 20000 $100 \sim 300$ 5 1 100 1000 20 1 1 Rope Granular 1000 20 1 100 1 200 3 5 **Block Pushing** 11000 4

Table 4: Dataset details and dataset specific configurations

A.1 Datasets and Environment Details

We elaborate various datasets and environments where our method is experimented on (Table 4). Offline trajectory datasets of Pointmaze, Wall, PushT, Granular and Rope as well as some of dataset-specific configurations are adopted from those provided by [7]³. Configurations specific to dataset include history trajectory length for the world model and frame skip length, which is an interval of frames to and from the world model, reducing redundancy between consecutive inputs. We also differ training epoch due to difference of dataset size and complexity.

Pointmaze. A navigation task introduced in D4RL [38] where an agent interacts with given 2D maze environment. There are 2000 trajectories with length of 100 created with random actions. Since we use task-agnostic world model with goal-conditioned planning, goal point is not visualized in each frame.

Wall. A visually simplistic 2D navigation task where an agent needs to pass a door to a separated room. There are 1920 trajectories with length of 50 created with random actions.

PushT. A 2D control task introduced in [39] where an agent needs to manipulate T-shaped block to a designated location. Dataset is generated by rollouting expert demonstration action trajectory with additional action noise in the environment. This allows the world model to learn various dynamics.

Granular and Rope. Fine-grained manipulation tasks involving deformable objects introduced in [40]. Both datasets have 1000 trajectories with length of 20 created with random actions.

Block Pushing. Robotics control task requiring precise spatial reasoning to position blocks correctly. We generate 11000 trajectories following PushT generation process.

A.2 Main Method Implementation Details

Our model is built on a pre-trained DINO [3] ViT backbone which is frozen during training. Specifically, we utilize DINO-ViT-S/16 on 224x224 image, which creates a 14x14 spatial tokens per image. Visual tokens from context frames are flattened as a input to the world model. Actions and proprioceptive vectors are linearly projected on a dimension of 10 respectively and concatenated to every visual token along the feature dimension axis. The world model is a causal transformer decoder, which predicts the tokens of the next timestep. The transformer has 6 attention layers, 16 attention heads per layer, and 2048 embedding dimensions. The world model is trained with Adam optimizer at a learning rate of 5e-4 without scheduler for 100 epochs, batch size of 32, dropout probability of 0.1. All experiments were conducted using at most 4 Nvidia RTX 3090s.

MPC rollouts utilize the Cross-Entropy Method (CEM) with action distribution defined as a Gaussian distribution. CEM is performed with planning horizon of 5, optimizing by mean and variance of top-10 action sequences among 100 candidate sequences. CEM optimization is done for 10 iterations and returns the mean of the action distribution as the final action sequence, executing all the planned action sequence for every MPC step. MPC iterates until the task is completed or until it reaches a maximum limit of 10 iterations.

³https://github.com/gaoyuezhou/dino_wm

A.3 HSIC Analysis Details

Hilbert–Schmidt Independence Criterion (HSIC). We measure statistical dependence between two random variables X and Y using the Hilbert–Schmidt Independence Criterion (HSIC) [30], defined via kernels k and ℓ on their respective domains. Let K and L be the $n \times n$ Gram matrices with entries $K_{ij} = k(x_i, x_j)$ and $L_{ij} = \ell(y_i, y_j)$, and $H = I_n - \frac{1}{n} \mathbf{1} \mathbf{1}^{\top}$ the centering matrix. Then the empirical HSIC is

$$\widehat{\mathrm{HSIC}}(X,Y) = \frac{1}{(n-1)^2} \operatorname{tr}(KHLH),$$

and we normalize it as

$$\mathrm{nHSIC}(X,Y) = \frac{\widehat{\mathrm{HSIC}}(X,Y)}{\sqrt{\widehat{\mathrm{HSIC}}(X,X)\,\widehat{\mathrm{HSIC}}(Y,Y)}},$$

so that $nHSIC \in [0, 1]$, with 0 indicating independence and 1 maximal dependence.

Experimental Setting. We compute nHSIC between visual tokens and corresponding environment state vectors under varying dropout probabilities. A single dropout mask is fixed within each batch of size n=128. Then, we repeat with 20 independent masks of same dropout rate and report the mean nHSIC. Visual tokens use a linear kernel, while state vectors use an RBF kernel whose bandwidth is set by the median heuristic. We utilized state vectors from the Granular dataset, consisting of the x and y coordinates for 12,774 particles.

A.4 Attentive Probing Details

Attentive Probing. Attentive probing is a nonlinear probing method priorly used for downstream tasks since visual tokens do not satisfy linear separable guarantee. We use attentive probing to fairly compare predictive power of varying number of tokens. Instead of linear probing, attentive probing uses cross-attention layer to pool all input features to a single learnable query vector. After query residual connection, output is fed into 2-layer MLP with GeLU and LayerNorm, projecting to original input dimension. Then, final linear layer predicts the given probing target.

Experimental Setting. Using attentive probing to predict the environment state with visual tokens under varying dropout probabilities, we present the mean and standard deviation of validation loss when training the model for 5 times with different dropout masks for each dropout rate. We also add leave-1 case where extreme dropout is performed to leave only a single random visual token. We use feature dimension of 384 and 4 heads for the cross-attention layer and hidden dimension of 4 times the feature dimension for the MLP layer. We trained the probing module for 500 epochs. The optimization was performed using Adam with a learning rate of 1×10^{-5} and a batch size of 128, incorporating a cosine scheduler and omitting a warmup period. Parallel to our HSIC analysis, we used Granular dataset state information. Rather than attempting to precisely predict 12,774 particle locations (impractical due to the order of particles and dimensionality), our probing module predicts the mean and standard deviation of x and y coordinates for all particles, thereby estimating their approximate position and spread as state information.

A.5 Token Selection Methods Details

LTRP. LTRP (Learning to Rank Patches; [21]) utilizes a pre-trained MAE (Masked Autoencoder; [36]) to learn a ranking model that assesses the importance of individual patch tokens. With 90% of the patch tokens masked, LTRP compares the reconstruction results (using L_1 distance) when each remaining token is individually removed versus when it is retained. Tokens contributing more significantly to the reconstruction error are considered more important. The ranking model is trained using ListMLE [41], optimizing the order of the top 20 items within each list. For the ranking model, we employed a ViT-Small architecture, while the MAE utilized a ViT-Base checkpoint. The ranking model was trained on ImageNet-1K for 50 epochs using four NVIDIA RTX 3090 GPUs. For aspects not explicitly mentioned, training configurations adhered to the defaults outlined in the original paper. The LTRP code is available here⁴, and the MAE ViT-Base checkpoint is from here⁵.

⁴https://github.com/irsLu/ltrp

⁵https://github.com/facebookresearch/mae

Attention-Encoder. Similar to [23, 24, 25], we gauge token importance by examining the attention map between the CLS token and other patch tokens within a pre-trained DINO encoder. Tokens receiving higher attention weights from the CLS token are deemed most significant. We implement token dropping by retaining the top-K tokens sorted by their attention weights. Our experiments utilized the DINO-ViT-S/16 checkpoint⁶, specifically leveraging the attention map from the final transformer block of the DINO encoder.

STAR. STAR (SynergisTic pAtch pRuning; [25]) determines a comprehensive importance score for each layer by combining two distinct components: an intra-layer importance score, derived from the attention weights between the CLS token and individual patch tokens, and an inter-layer importance score, quantified using Layer-wise Relevance Propagation (LRP). The inter-layer scores were pre-computed on the ImageNet-1K dataset, consistent with the methodology outlined in the original publication. Given that the original STAR implementation was based on DeiT, we modified their codebase to ensure compatibility with DINO. The aggregated score for layer l, denoted S_l , is formulated as $S_l = S_l^{\text{intra}^{\alpha}} \times S_l^{\text{inter}^{(1-\alpha)}}$. We set $\alpha = 0.3$, which is one of the values proposed in the original paper. Analogous to the Attention-Encoder strategy, token dropping was realized by sorting tokens according to their scores from the final encoder layer in descending order and preserving only the top-K. The official code of STAR can be found here 7 .

Attention-WM. Unlike encoder-based methods like Attention-Encoder, this approach stems from the idea that it might be more efficient to retain tokens deemed important by the world model during dynamics prediction for a given action. Thus, we leverage the attention maps from our trained ViT-based world model. Since our world model does not utilize a CLS token, we instead consider the attention maps involving all individual patch tokens. Specifically, for each patch token acting as a key, we calculate the average attention it receives from all query patch tokens. We then assume that tokens with higher average attention are more important. A drawback of this method is the two-pass forward computation during planning. First, the world model must be forwarded with all tokens to obtain the attention maps across all layers. These maps are then used as importance scores to select the most significant patch tokens. Subsequently, a second forward pass is executed with only the selected tokens, introducing an additional computational cost. In this approach, we averaged attention maps across all layers.

Agglomerative Token Clustering (ATC). Inspired by [28], we employ a modified version of Agglomerative Token Clustering (ATC) for our clustering approach. Necessary modifications were made as the original ATC was primarily designed for single-frame applications, such as classification or segmentation. Adapting it for goal-conditioned world model-based planning necessitated a modified mechanism to address multiple history frames, and to match clusters between the goal image features and predicted latent features.

Our clustering methodology proceeds as follows. First, we extract DINO features from the input image and apply agglomerative clustering using either L_2 distance or cosine similarity (the choice between these two metrics did not significantly affect results). The number of clusters is dynamically determined by the desired drop ratio (e.g., 137 clusters for a 20% drop). Using the cluster assignments from the initial frame as anchors, subsequent frames undergo K-means clustering. After clustering, patches within each cluster are aggregated via average pooling, maintaining the same number of patches as clusters. To address inconsistencies in clustering results across visually similar scenes, we observed through trial and error that storing and re-using K-means centroids from the previous frame as initial centroids for the subsequent frame ensures better consistency by aligning clusters across consecutive frames.

To integrate this into MPC, we initially cluster the goal image and use it as an anchor for clustering the current observation, aiming for inherent cluster alignment. However, this alone did not guarantee perfect alignment, especially with an increased number of clusters. To mitigate this, we introduced an additional matching step: during the loss calculation within the CEM, specifically when selecting the top-K actions, we employ Hungarian matching between the world model's predictions and the goal clusters to ensure proper alignment. Without this crucial matching step, we observed that the results degrade significantly. For instance, in the Wall Environment, using 128 clusters, experiments

⁶https://github.com/facebookresearch/dino

⁷https://github.com/LannWei/STAR_ICLR

over 30 episodes showed that the success rate improved from 70.0% without matching to 86.7% with matching applied.

B Additional Experiments

B.1 Grouped Attention

This section investigates the influence of randomized grouped attention (applied during training) on world model prediction error during planning, relative to full attention (Fig. 8). The analysis spans multiple datasets and various dropout ratios. In contrast to the main text's primary focus on findings for the Wall dataset under a 50% dropout condition, the present discussion offers a more comprehensive overview of results across these diverse conditions. We quantify this impact by presenting the mean relative L_2 distance of retained tokens on the validation set of each dataset, both with and without dropout, for each attention mechanism. This metric normalizes the L_2 distance by the tokens' norm. All reported values represent the mean and standard deviation derived from five independent experiments. Our analyses consistently demonstrate that grouped attention leads to lower prediction error and reduced variance compared to full attention across the Wall, Granular, Rope, and Block Pushing datasets. We observe an apparent correspondence between these improvements and notable enhancements in success rates across the evaluated datasets (as detailed in the main text). This observed pattern seems to hold for a majority of the dropout ratios investigated.

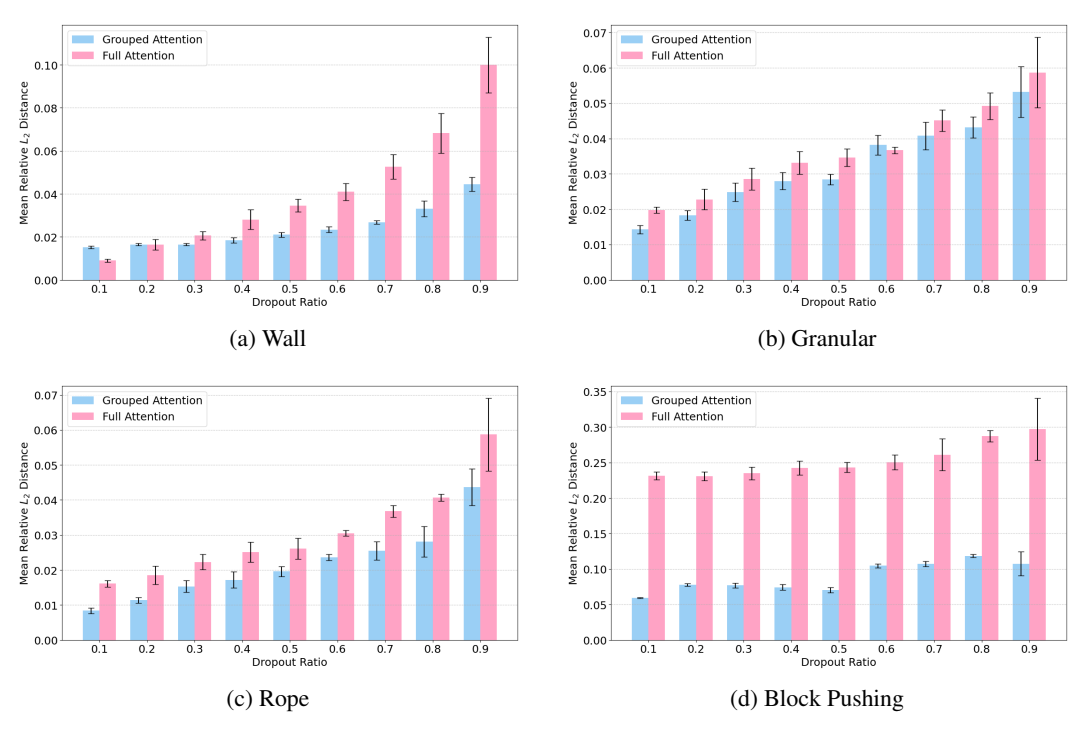


Figure 8: Contribution of grouped attention during pretraining to planning on various drop ratios across various datasets.

B.2 Planning Robustness to Noises

In this section, we experimentally validate our claim that the remaining prediction error, consistent with prior studies on CEM's robustness to noise and uncertainties, is sufficient for effective planning. To investigate this, we first examined whether the prediction error, incurred by token dropping in the world model, correlates with the world model's input across different dropout ratios. We reduced the high-dimensional input features to a 2D representation using UMAP and generated a scatter plot comparing these UMAP coordinates with the magnitude of the error (Frobenius norm) (Fig. 9).

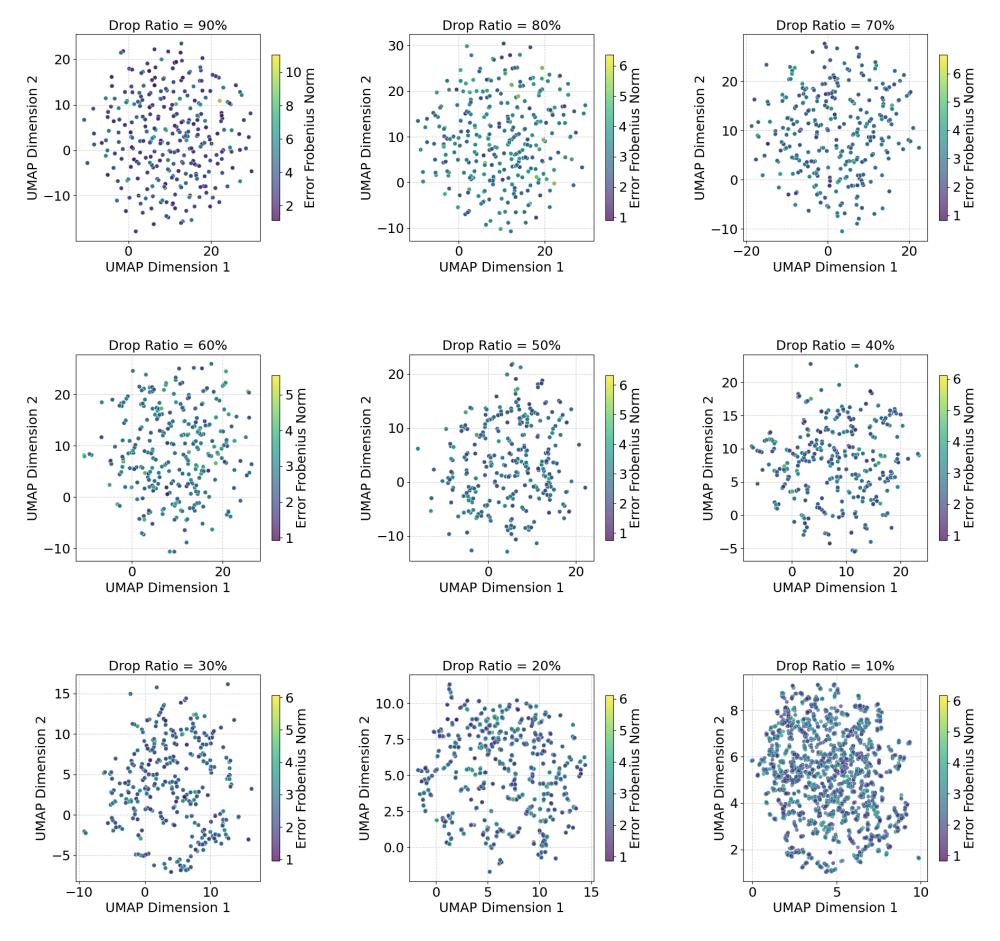
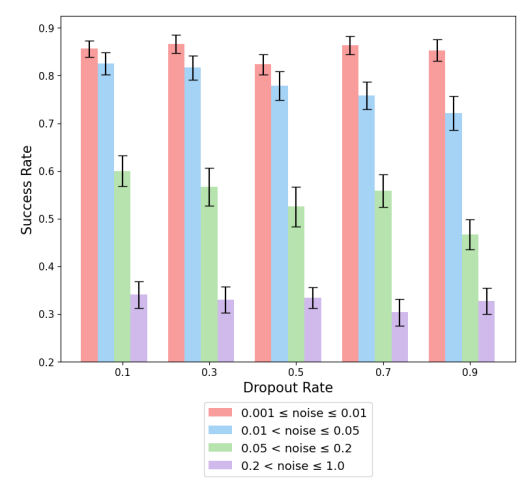


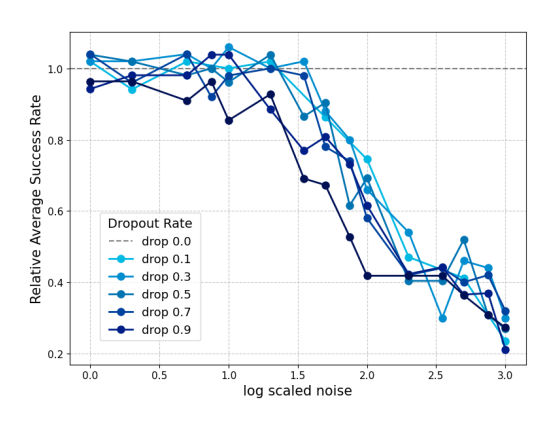
Figure 9: Scatter plots visualizing the embedding of world model inputs in a 2D UMAP manifold, colored by their prediction error magnitude (Frobenius norm), presented across different token drop ratios.

Visual inspection of the UMAP projection of input features shows no obvious global or local patterns linking UMAP coordinates of model inputs to the error norm. Data points, colored by their error magnitude (Frobenius norm), are generally intermixed throughout the low-dimensional embedding. Therefore, this specific UMAP representation of input features, based on visual analysis, does not clearly indicate a strong, direct relationship between the spatial embedding of these features and their corresponding error magnitude.

Given the findings, we assume that the prediction error inherent in world model when operating on token subsets could be approximated as zero-mean Gaussian noise, exhibiting no direct correlation with the input tokens. To empirically test the robustness of MPC-CEM planning, we proceeded to add this synthesized noise to the input tokens during the actual planning.

To simulate the behavior of a dropout-affected world model, we begin by generating predictions using the full world model without applying dropout. Next, we modify these predictions by randomly dropping a subset of the predicted tokens and adding zero-mean Gaussian noise to the remaining ones. These modified predictions are then used for MPC-CEM planning. The magnitude of the Gaussian noise was scaled relative to the token norm and experimented under varying noise scales and dropout rates. We then evaluated the robustness of MPC-CEM planning by measuring the success rates of actual rollouts in the environment using these noisy predictions. This experiment was conducted in the point maze environment, with the agent allowed a maximum of 3 MPC planning steps per episode. The presented success rates were averaged over 60 independent evaluations.





- (a) MPC-CEM success rate vs. dropout rate under various noise conditions.
- (b) Relative MPC-CEM success rate vs. log noise scale for different dropout ratios.

Figure 10: Robustness of MPC-CEM planning to prediction dropout and noise. The results show minimal degradation of success rates by increasing dropout rates and performance loss only after a certain noise threshold.

Table 5: Comparison of planning time and change across different drop ratios (compression rates) between drop and clustering apporaches.

| | Pointmaze Wal | | | Wall | PushT | | | | Block Pushing | | | |
|----------------------------------|---------------|------------------------------|------------|------|------------------------------|------------|-----|-------------------------------|---------------|-----|------------------------------|-----------------|
| Drop Ratio (Compression Rate) | | ng Time (iter) Cluster | Change (%) | | ng Time (iter) Cluster | Change (%) | | ing Time /iter) Cluster | Change (%) | | ng Time /iter) Cluster | Change - (%) |
| 10% | 165 | 332 | +101.2 | 73 | 246 | +237.0 | 149 | 328 | +120.1 | 278 | 478 | +71.9 |
| 20% | 141 | 297 | +110.6 | 69 | 235 | +240.6 | 131 | 295 | +125.2 | 259 | 444 | +71.4 |
| 30% | 126 | 269 | +113.5 | 65 | 235 | +261.5 | 114 | 267 | +134.2 | 240 | 407 | +69.6 |
| 40% | 106 | 245 | +131.1 | 62 | 207 | +233.9 | 97 | 237 | +144.3 | 214 | 376 | +75.7 |
| 50% | 93 | 214 | +130.1 | 53 | 192 | +262.3 | 82 | 213 | +159.8 | 208 | 359 | +72.6 |
| 60% | 80 | 193 | +141.3 | 50 | 184 | +268.0 | 69 | 187 | +171.0 | 200 | 318 | +59.0 |
| 70% | 69 | 172 | +149.3 | 46 | 164 | +256.5 | 59 | 170 | +188.1 | 184 | 295 | +60.3 |
| 80% | 56 | 152 | +171.4 | 46 | 145 | +215.2 | 49 | 139 | +183.7 | 175 | 266 | +52.0 |
| 90% | 48 | 137 | +185.4 | 42 | 117 | +178.6 | 38 | 115 | +202.6 | 167 | 248 | +48.5 |

The results (Fig. 10) indicate that MPC-CEM planning sustains effective performance at dropout levels with minimal performance decrease, which aligns with our main experiments. While its performance remains stable as noise levels increase up to a specific threshold, beyond which it begins to decline. This suggests that MPC-CEM is robust to prediction errors caused by token dropout, reinforcing our claim that manageable for planning. These observations also align with prior works on the resilience of CEM to noise and uncertainties.

B.3 Dropout vs. Clustering in Execution Times

Table 5 compares the execution times of single MPC iterations between dropout and clustering methods at various compression rates (drop ratios). The clustering approach requires additional computations, including the calculation of pairwise distances or similarities among patches, incurring a quadratic complexity relative to the number of clusters. Furthermore, since clustering merges patches from multiple spatial locations, the resulting pooled features lose fixed spatial positions, necessitating additional matching procedures when computing distances between goal image patches and observations during MPC planning. Consequently, the clustering method requires significantly more computation, with runtime increases of up to 268.0% compared to dropout, as shown in Table 5. In contrast, our dropout approach merely samples patch indices, which results in nearly constant computational overhead regardless of dropout ratio. Additionally, since the same patch subsets

are consistently applied to both observation and goal images, the spatial positions remain fixed, eliminating the need for extra matching processes.

C Visual Demonstations

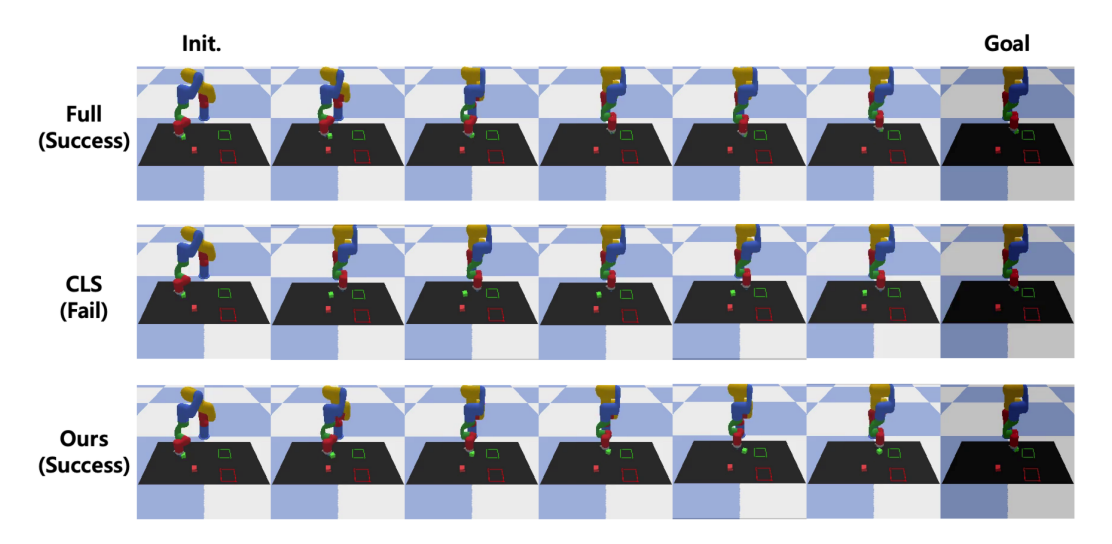


Figure 11: Rollout demonstration on Block Pushing environment of Full, CLS, and our methods (60% Drop).

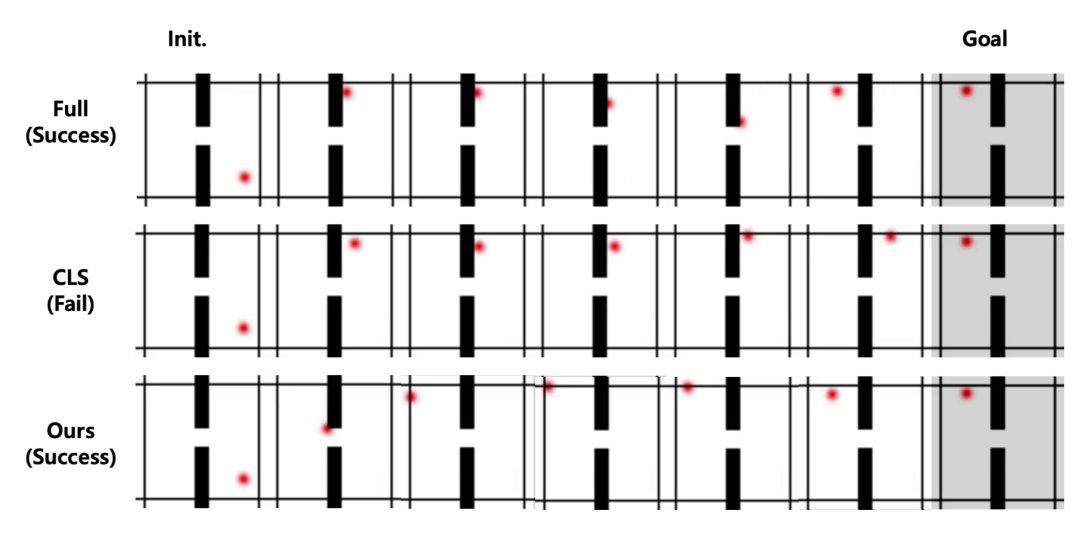


Figure 12: Rollout demonstration on Wall environment of Full, CLS, and our methods (50% Drop).